Supporting Information

Selective intracellular free radical generation against cancer cells by bioactivation of low-dose artesunate with functionalized mesoporous silica nanosystem

*Jingke Fu, Yiran Shao, Chao Shi, Wenbo Bu and Yingchun Zhu**

Key Lab of Inorganic Coating Materials, Shanghai Institute of Ceramics, Chinese Academy of Sciences, Shanghai 200050, China.

* To whom correspondence should be addressed: Tel.: 86-21-52412632; Fax: 86-21-52412632; E-mail: yzhu@mail.sic.ac.cn.

Experimental section

Materials

Cetyltrimethyl ammonium bromide (C_{16}TAB), tetraethyl orthosilicate (TEOS), iron(II) sulfate heptahydrate ($FeSO_4 \cdot 7H_2O$) and hydrogen peroxide (H_2O_2, 30% in water) were obtained from Sinopharm Chemical Reagent Co., Ltd. 3-aminopropyltriethoxysilane (APTES), Dimethyl sulfoxide (DMSO), 3-(4,5-dimethylthiazol-2-yl)-2,5-diphenyltetrazolium bromide (MTT), safranine, fluorescein isothiocyanate (FITC), paraformaldehyde (PFA) and artesunate (ART) were purchased from Sigma-Aldrich. Phosphate buffered saline (PBS, pH 7.4), RPMI-1640 medium, trypsin and fetal bovine serum (FBS) were obtained from Gibco. All chemicals were used without further purification. Ultrapure water was used throughout all the experiments.

Synthesis of Hollow Mesoporous Silica Nanospheres and Loading of Artesunate (ART@HMS)

Firstly, hollow mesoporous silica nanospheres (HMS) were prepared according to the literature procedure.[1] After removing the templates by an ion-exchange procedure,[2] the obtained products were referred as HMS. Then, artesunate (ART) was loaded into HMS by wet impregnation. The as-prepared HMS (10 mg) were dispersed into ART acetone solution (0.4 mg mL^{-1}, 6 mL) and stirred in the dark for 24 h. Then, the solid was collected by centrifugation, washed with water, and freeze dried. The obtained white powder was referred as ART@HMS. The ART loading efficiency in ART@HMS was

Synthesis of FITC-Labeled ART@HMS (ART@HMS-FITC)

Fluorescein isothiocyanate (FITC) was reacted with 3-aminopropyltriethoxysilane (APTES) in methanol under dark conditions to obtain FITC-APTES. Then, ART@HMS (50 mg) were dispersed into the FITC-APTES solution (3 mL) and stirred in the dark for 12 h. The FITC-conjugated ART@HMS (ART@HMS-FITC) were collected by centrifugation, washed with methanol, and dried under vacuum in the dark.

Synthesis of Fe/O Clusters-Mesoporous Silica Nanosystem (Fe/O-MSN)

The synthetic procedure for Fe/O-MSN involves two steps. Firstly, mono-dispersed mesoporous silica nanoparticles (MSN) were prepared by base-catalyzed condensation reaction as described in the literature.[3] The obtained templates (C_{16}TAB)-containing product was denoted as MSN-C. Afterwards, Fe/O clusters were introduced into the mesoporous channels of MSN by using Fenton's reagent (Fe^{2+}-H_2O_2) as the iron precursor based on the reported methods.[4,5] Briefly, the as-prepared MSN-C (0.3 g) was suspended into deionized water (20 mL) under ultrasonic treatment. The obtained suspension was transferred into a two-necked flask equipped with a condenser and incubated at 0 °C in an ice bath. $FeSO_4$ aqueous solution (0.6 M, 10 mL) was then quickly added into the above suspension. Immediately, H_2O_2 (30%, 10 mL) was added to this suspension dropwise. Once the Fenton reaction occurred, the solution turned puce and the removal of the templates (C_{16}TAB) was visually observed by the gush of abundant spume out of the flask. The reaction was stopped after another 2 h. The obtained solid was collected by centrifugation, washed with water and ethanol, and freeze dried. Finally, the dry solid was calcined at 300 °C for 30 min to obtain Fe/O-MSN.

Supplementary Figures

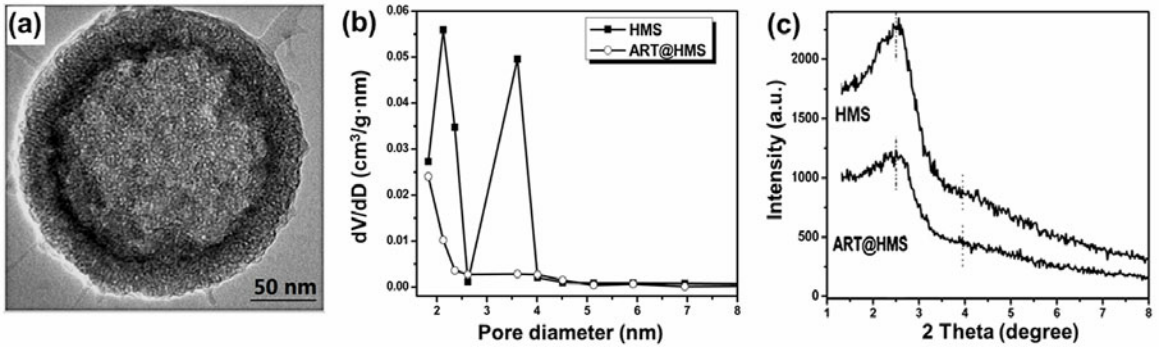

Fig. S1 Characterization of the as-prepared HMS and ART@HMS. (a) Highly magnified TEM image of HMS. (b) BJH pore size distribution plots and (c) small-angle XRD patterns of the HMS and ART@HMS. The pore size of HMS is centered at 2.2 nm and 3.6 nm, and decreases to 1.7 nm after the ART loading. The as-prepared HMS present a definite diffraction peak at 2.5° (2θ) with a broad shoulder peak around 3.9°, demonstrating the well-defined wormlike mesostructure. After the ART loading, the XRD pattern of ART@HMS is almost consistent with that of the HMS matrix, indicating that the mesostructure is well kept in the ART@HMS.

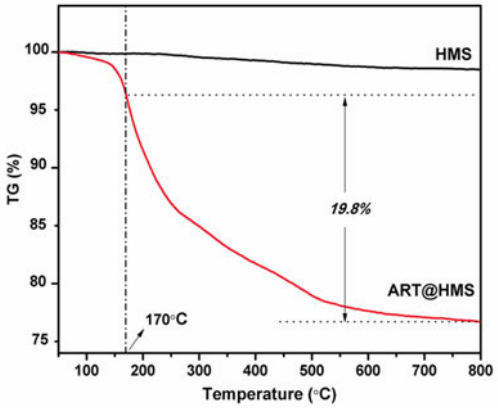

Fig. S2 TGA curve of HMS and ART@HMS. The weight loss is 1.46% in HMS (absorbed physical water) and is 19.8% in ART@HMS. The ART loading amount was determined to be 18.34% by subtracting the weight loss of HMS from the ART@HMS.

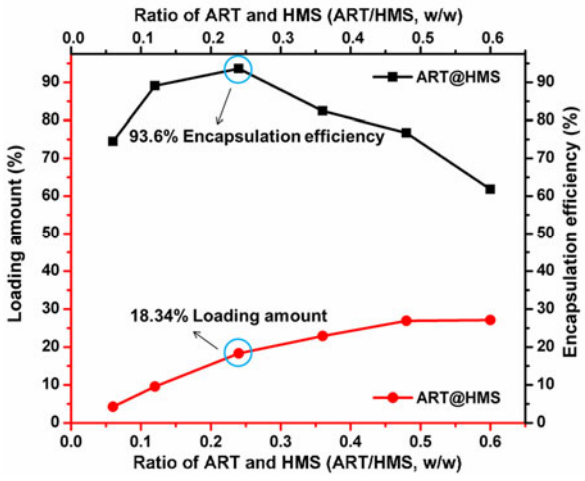

Fig. S3 Loading amount and encapsulation efficiency of ART in HMS with different ART/HMS ratios (w/w). The as-prepared HMS was dispersed into ART acetone solution with different concentrations. After stirring for 24 h in the dark, the ART-loaded HMS (ART@HMS) were collected by centrifugation. To evaluate the ART encapsulation efficacy, the supernatant ART solution

was collected and the residual ART content was measured by HPLC (λ = 210 nm). The encapsulation efficiency (EE) of ART in HMS was calculated as follows: EE = $(W_i\text{-}W_r) \times 100\%/W_i$ (W_i: initial ART amount; W_r: residual ART amount). Following the curves, we prepared the ART@HMS with an ART/HMS ratio of 0.24. The obtained ART loading amount and encapsulation efficiency is 18.34% and 93.6%, respectively.

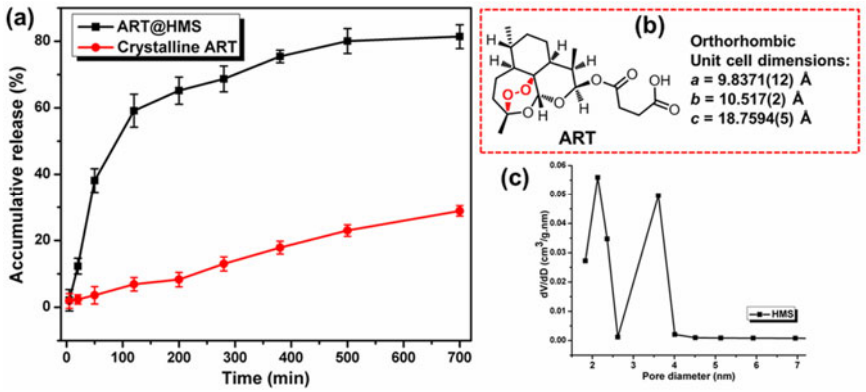

Fig. S4 (a) Release profile of ART from ART@HMS and crystalline ART in PBS (pH 7.4) under sink condition, which was accomplished by adding 0.2% (w/v) sodium lauryl sulfate (SLS) to the PBS release media. The depicted results were represented as means ± SDs (n = 3). The encapsulation of ART in HMS could remarkably improve the ART dissolution rate in aqueous medium, which is beneficial to its pharmaceutical performance and bioavailability. (b) Chemical structure and crystallographic data of ART. (c) Pore size distribution of HMS. The molecule size of ART was smaller than the pore size of HMS (*ca.* 2.8 and 3.6 nm), which guarantees the sustained release of ART from the HMS.

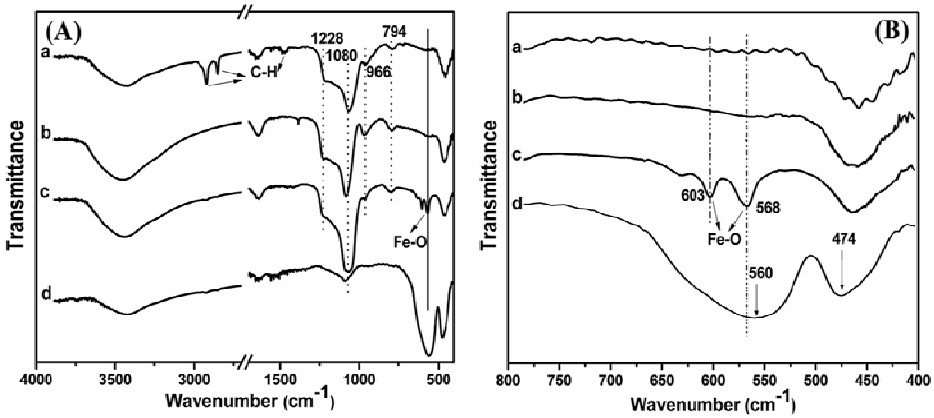

Fig. S5 (A) FTIR spectra (4000-400 cm^{-1}) of (a) templates-containing mesoporous silica (MSN-C), (b) templates-free mesoporous silica (MSN), (c) Fe/O-MSN and (d) commercial Fe_2O_3 NPs. (B) Magnified FTIR spectra (800-400 cm^{-1}) of (a) MSN-C, (b) MSN, (c) Fe/O-MSN and (d) commercial Fe_2O_3 NPs.

Discussion: As shown in Figure S5A, both the templates-containing mesoporous silica (MSN-C) and the templates-free mesoporous silica (MSN) show characteristic bands of mesoporous silica at 1228, 1080, 966 and 794 cm^{-1}, which are attributed to the asymmetric stretching vibration of Si-O-Si (1228 and 1080 cm^{-1}), the symmetric stretching vibrations of Si-O-Si (794 cm^{-1}) and the stretching vibration of Si-OH (966 cm^{-1}),[6] respectively. Besides, the C-H stretching vibrations at 2850-2900 cm^{-1} and C-H bending/deformation vibrations at 1240-1500 cm^{-1} are clearly observed in MSN-C (Figure S5A-a), but not in MSN (Figure S5A-b) and Fe/O-MSN (Figure S5A-c), indicative of the complete remove of templates in the MSN and Fe/O-MSN. It's noteworthy that the characteristic bands of mesoporous silica at 1228, 1080, 966 and 794 cm^{-1} are also observed in Fe/O-MSN, demonstrating the chemical stability of the MSN and the mesopores preservation in Fe/O-MSN. In addition, magnified-FTIR spectra (800-400 cm^{-1}) were analyzed to clarify the structure difference of the samples (Figure S5B). In contrast to the MSN, two moderate bands at 603 and 568 cm^{-1}, due to the Fe-O vibrations of iron oxide,[7,8] appear in Fe/O-MSN (Figure S5B-c). Unlike the commercial Fe_2O_3 NPs

(*ca.* 30 nm, Figure S5B-d), which display broad absorption centered at 560 and 474 cm^{-1}, the Fe/O-MSN absorption shifts to higher frequencies. It is reported that the IR spectra of particles are associated with their particle size/shape and the principal IR absorption shifts to lower frequency with increasing particle size.[9] We speculate that smaller Fe/O clusters are formed in the Fe/O-MSN due to the confinement effect of the mesoporous silica matrix.

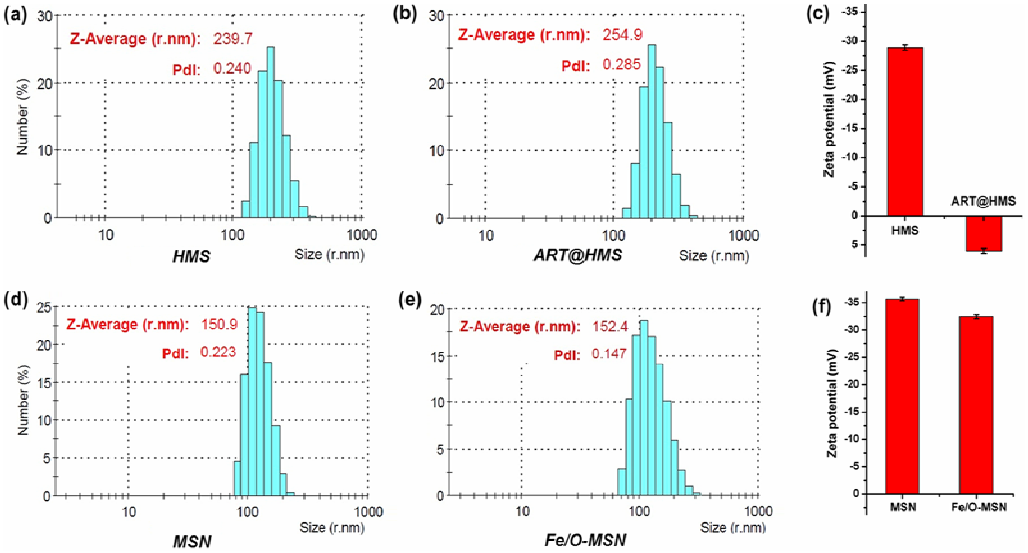

Fig. S6 Dynamic light scattering **(**DLS) particle size distributions of (a) HMS, (b) ART@HMS, (d) MSN and (e) Fe/O-MSN. Zeta potentials of (c) HMS, ART@HMS and (f) MSN, Fe/O-MSN. The hydrodynamic size of HMS (*ca.* 240 nm) and ART@HMS (*ca.* 255 nm) show a little increase than that obtained from the TEM observation (*ca.* 220 nm) due to the interaction between the nanoparticles and the water molecules. Similar results were obtained in the MSN and Fe/O-MSN (Fig. S6d,e). Besides, all the nanoparticles show well polydispersity with PDI < 0.3. Zeta potential analysis shows that the HMS exhibited a negative potential of about -28.9 mV while the zeta potential of ART@HMS increased to +6.01 mV. Considering the fact that cancer cell surface is negatively charged,[10] ART@HMS would more easily bind to cancer cell membranes, which further led to more efficient cargo delivery. In addition, both the Fe/O-MSN and MSN exhibited negative potentials of above -30 mV. It's reported that nanoparticles with a zeta potential above (+/-) 30 mV are stable in suspension,[11] which indicates the as-prepared MSN and Fe/O-MSN exhibited stable aqueous dispersion in physiologic environment.

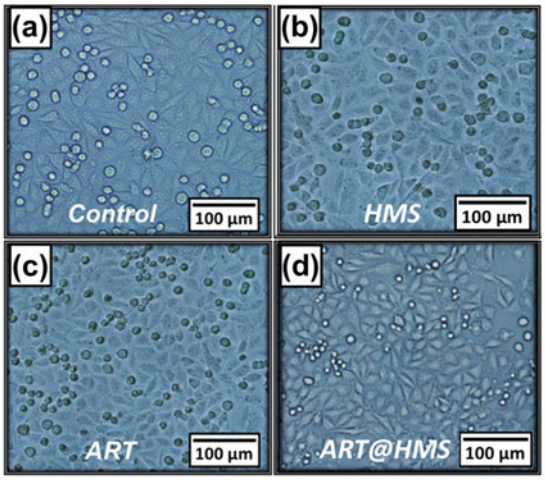

Fig. S7 Microscopic images of ZR75-30 cells after 24 h exposure to (a) fresh culture media without samples (negative control), (b) HMS (200 μg mL^{-1}, toxicity control), (c) free ART (12 μM) and (d) ART@HMS (containing 12 μM ART). It's clear that the cells exposed to free ART and ART@HMS are well kept with favorable adherence, indicating that the low-dose ART and ART@HMS *per se* are innocuous.

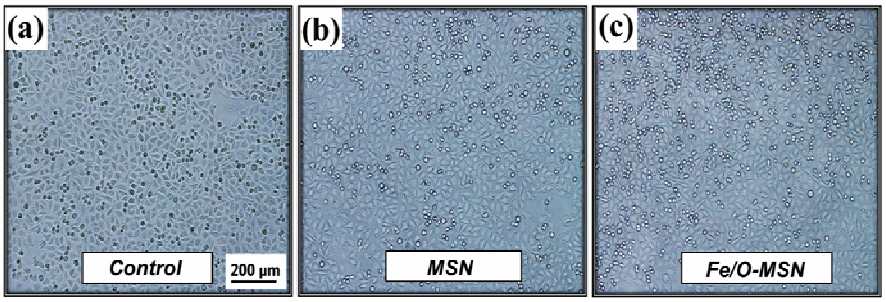

Fig. S8 Microscopic images of ZR75-30 cells after 24 h exposure to (a) fresh culture media (negative control), (b) MSN (100 μg mL^{-1}, toxicity control) and (c) Fe/O-MSN (containing 80 μM Fe). The scale bar in (a) applies to all panels. Cells in all groups are spindly and grow with favorable adherence after 24 h culture, demonstrating that the Fe/O-MSN are biocompatible and play no toxic effect to ZR75-30 cells.

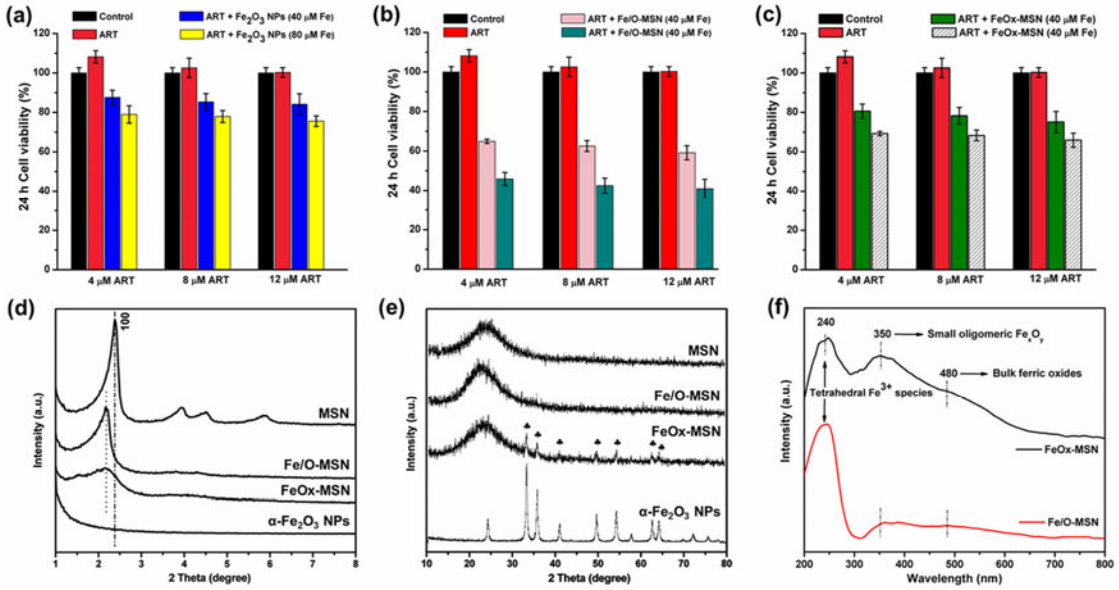

Fig. S9 *In vitro* cytotoxicity of (a) free ART + free α-Fe_2O_3 NPs, (b) free ART + Fe/O-MSN and (c) free ART + FeOx-MSN against ZR75-30 cells after incubation in RPMI-1640 media for 24 h. Culture media without samples were used as the negative controls. All results are represented as means ± SDs (n = 6). (d) Small-angle XRD patterns of the as-prepared MSN, Fe/O-MSN, iron oxides-loaded MSN (FeOx-MSN) and commercial α-Fe_2O_3 NPs. (e) Wide-angle XRD patterns of the MSN, Fe/O-MSN, FeOx-MSN and α-Fe_2O_3 NPs. (f) UV-visible diffuse reflection spectra (UV/vis DRS) of Fe/O-MSN and FeOx-MSN.

Discussion: Free ART + commercial free α-Fe_2O_3 nanoparticles (NPs, 30 nm) were used as a reference to evaluate the efficacy of the reported "pro-drug" nanosytem (Fig. S9a). Besides, cells were also incubated with free ART + free Fe/O-MSN for comparison (Fig. S9b). It can be seen that the cytotoxicity sensitizing effect of free α-Fe_2O_3 NPs is obviously lower than that of Fe/O-MSN with equivalent Fe concentration of 40 and 80 μM. To further investigate the superiority of the high-dispersed Fe/O clusters in the MSN, iron oxides-loaded MSN (referred as FeOx-MSN), which were prepared by conventional wet impregnation method, were used for comparison. As shown in Fig. S9b,c, the Fe/O-MSN exhibit more significant cytotoxicity-sensitizing effect compared with FeOx-MSN with equivalent Fe concentration of 40 and 80 μM. As can be seen from the XRD data in Fig. S9d,e, much smaller and well-dispersed amorphous Fe/O species are formed in the Fe/O-MSN whereas α-Fe_2O_3 crystals larger than the pore sizes of MSN are formed in the FeOx-MSN. It's speculated that the smaller and well-dispersed Fe/O species in the mesoporous channels of Fe/O-MSN would facilitate their heterogeneous reaction with the ART. Furthermore, as can be seen from the UV/vis DRS in Fig. S9f, the Fe/O-MSN contain more isolated framework tetrahedral Fe^{3+} species[12] and are free from bulk ferric oxides. In contrast, the UV/vis DRS of FeOx-MSN shows evident presence of oligomeric iron oxides[13]and bulk ferric oxide

species.[4] It has been demonstrated that the isolated iron is much more active in catalytic reactions than the "bulklike" iron oxide NPs.[4,13] It can be inferred that the well dispersed isolated framework tetrahedral Fe^{3+} species in the Fe/O-MSN may lead to an increase in the number of active sites for the heterogeneous reaction.

References

1 X. L. Fang, C. Chen, Z. H. Liu, P. X. Liu and N. F. Zheng, *Nanoscale*, 2011, **3**, 1632-1639.

2 N. Lang and A. Tuel, *Chem. Mater.*, 2004, **16**, 1961-1966.

3 I. I. Slowing, B. G. Trewyn and V. S. Y. Lin, *J. Am. Chem. Soc.*, 2007, **129**, 8845-8849.

4 Y. M. Liu, J. Xu, L. He, Y. Cao, H. Y. He, D. Y. Zhao, J. H. Zhuang and K. N. Fan, *J. Phys. Chem. C*, 2008, **112**, 16575-16583.

5 J. L. Vennerstrom, S. Arbe-Barnes, R. Brun, S. A. Charman, F. C. K. Chiu, J. Chollet, Y. X. Dong, A. Dorn, D. Hunziker, H. Matile, K. McIntosh, M. Padmanilayam, J. S. Tomas, C. Scheurer, B. Scorneaux, Y. Q. Tang, H. Urwyler, S. Wittlin and W. N. Charman, *Nature*, 2004, **430**, 900-904.

6 Y. Chen, H. R. Chen, D. P. Zeng, Y. B. Tian, F. Chen, J. W. Feng and J. L. Shi, *ACS Nano*, 2010, **4**, 6001-6013.

7 Y. M. Zhao, Y. H. Li, R. Z. Ma, M. J. Roe, D. G. McCartney and Y. Q. Zhu, *Small*, 2006, **2**, 422-427.

8 J. S. Chang, Z. L. Kong, D. F. Hwang and K. L. B. Chang, *Chem. Mater.*, 2006, **18**, 702-707.

9 J. T. Luxon, D.J. Montgome and R. Summitt, *Phys. Rev.*, 1969, **188**, 1345-1363.

10 P. Chandra, H. B. Noh and Y. B. Shim, *Chem. Commun.*, 2013, **49**, 1900-1902.

11 S. A. Wissing, O. Kayser and R. H. Muller, *Adv. Drug Deliver. Rev.*, 2004, **56**, 1257-1272.

12 Y. Zhou, J. Yang, J. Y. Yang, F. N. Gu, Y. Wang and J. H. Zhu, *J. Mater. Chem.*, 2011, **21**, 13895-13901.

13 Y. Li, Z. C. Feng, H. C. Xin, F. T. Fan, J. Zhang, P. C. M. M. Magusin, E. J. M. Hensen, R. A. van Santen, Q. H. Yang and C. Li, *J. Phys. Chem. B*, 2006, **110**, 26114-26121.